Experimental Targeting and Control of Spatiotemporal Chaos in Nonlinear Optics

L. Pastur, L. Gostiaux, U. Bortolozzo, S. Boccaletti, and P. L. Ramazza
Istituto Nazionale di Ottica Applicata, Largo E. Fermi 6, 50125 Firenze, Italy
(Received 2 January 2004; published 5 August 2004)

We demonstrate targeting and control over spatiotemporal chaos in an optical feedback loop experiment. Different stationary target patterns are stabilized in real time by means of a two dimensional space extended perturbation field driven by an interfaced computer and applied in real space to a liquid crystal display device inserted within a control optical loop. The flexibility of the system in switching between different target patterns is also demonstrated.

DOI: 10.1103/PhysRevLett.93.063902 PACS numbers: 42.65.Sf, 05.45.Gg, 05.45.Jn, 47.54.+r

Control of complex dynamics refers to a process whereby the critical sensitivity of such dynamics to external disturbances is capitalized in order to select a proper tiny perturbation able to attain a desirable target behavior. In the last decade, a series of relevant issues such as stabilizing a given trajectory within an infinite set of unstable periodic orbits embedded within a chaotic attractor (*control of chaos*) or bringing a chaotic trajectory to a small neighborhood of some desired locations in phase space (*targeting of chaos*) have been addressed and solved in both low and high dimensional time-chaotic dynamics [1].

More recently, the interest switched to implementing control strategies for the stabilization of space-time-chaotic dynamics occurring in extended systems. In this latter framework, some theoretical attempts and numerical demonstrations have been offered for achieving control over one and two dimensional patterns [2], coupled map lattices and arrays of oscillators [3], or relevant model equations describing universal features of dynamics [4,5].

Reliable experimental control over space-time chaos (STC) remains however an open problem. In the field of nonlinear optics, a few experimental demonstrations of pattern control and targeting have been offered, based on filtering masks placed in a Fourier plane [6,7]. These methods provide a nice efficiency for the stabilization of stationary patterns with simple global symmetries, but their application to arbitrary target patterns is strongly limited by the practical difficulty of building suitable Fourier masks.

In this Letter we show the first experimental evidence of control of STC based upon a real-space real-time feedback technique, which is able to circumvent the above difficulties, thus allowing stabilization and targeting of two dimensional stationary patterns with arbitrary symmetries and shapes. This is realized by means of perturbations applied in the real space, and in times shorter than the characteristic time of the system dynamics, so that patterns of arbitrary complexity can be targeted and stabilized with good efficiency. We also show that our control strategy offers dynamical flexibility in switching from one to another target pattern, without the need of removing optical components (as, e.g., filters) in the control loop.

The experimental setup is sketched in Fig. 1(a). It consists of a main optical feedback loop (MOFL) hosting a liquid crystal light valve (LCLV) [8], and of an addi-

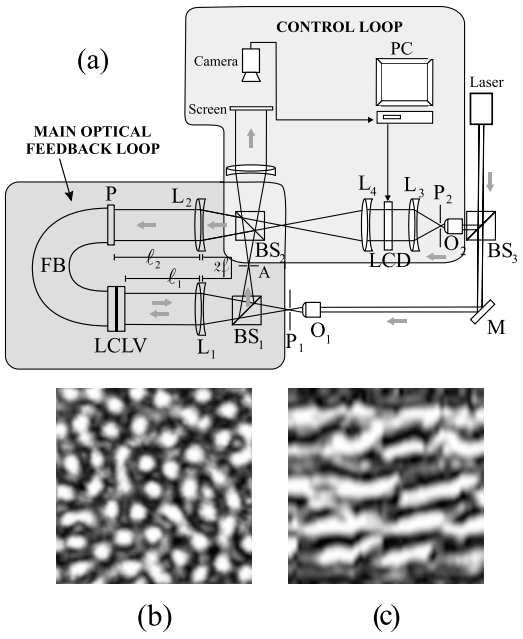

FIG. 1. (a) Experimental setup. Main loop: an extended laser beam is closed through a nonlinear Kerr-like medium (liquid crystal optical valve). Instabilities develop in the transverse plane of the beam. M: mirror, O_1: microscope objectives; P_1: pinhole; A: aperture; BS_1, BS_2: beam splitters; LCLV: liquid crystal light valve; L_1, L_2: lenses of focal lens f; FB: fiber bundle. In our experiment, the effective free propagation length is $2f - (l_1 + l_2) = +90$ mm. Control arm: O_2: microscope objectives; P_2: pinhole; BS_3: beam splitter; LCD: liquid crystal display; L_3, L_4: lenses. The arrows indicate the local direction of light propagation. (b) Snapshot of the uncontrolled STC state obtained for an input intensity $I/I_c \sim 3.2$ (I_c being the critical value for pattern formation from the uniform state to hexagons). The pattern intensity has been coded into a 256 level gray scale. (c) Space (vertical) time (horizontal) dynamical evolution of the central vertical line of pixels of Fig. 1(b).

 0031-9007/04/93(6)/063902(4)$22.50

tional electro-optic control loop. The latter consists of a video camera, a personal computer (PC) driving a liquid crystal display (LCD), and a laser beam which traverses the LCD before being injected into the MOFL. The LCLV operates as a Kerr-like medium, i.e., it induces on the reading light a phase delay proportional to the writing intensity, over the range of input intensities used in the experiments here reported. The LCD, operating in transmission, encodes linearly the gray level images output by the PC, onto the laser beam traversing it.

When the control loop is open, a homogeneous wave is sent onto the front face of the LCLV, and is reflected acquiring a spatial phase modulation. The diffractive propagation of this beam trough the MOFL converts the phase into amplitude modulations. In these conditions, the dynamics within the MOFL is described by the equation [9,10]:

$$\frac{\partial \phi}{\partial t} = -\frac{1}{\tau}(\phi - \phi_0) + D\nabla^2\phi + \alpha I_{fb}, \qquad (1)$$

where $\phi(x, y)$ is the phase of the optical beam at the output of the valve, τ is a relaxation time, D a diffusion coefficient, α the nonlinearity strength of the LCLV, ϕ_0 is the working reference phase, and $I_{fb}(x, y)$ is the feedback intensity impinging at the rear side of the valve.

The feedback intensity is a nonlinear (and nonlocal) function of the phase ϕ [9,10]. On increase of the pump intensity I, the homogeneous solution destabilizes, resulting in hexagonal patterns close to threshold. If the pump is further increased, regular hexagons lose stability in favor of space-time-chaotic dynamics [9,11]. Together with the pump value, another parameter of the utmost importance is the spatial frequency bandwidth of the system [7], controlled by the aperture A in Fig. 1. This aperture is located in a Fourier plane of the MOFL, and plays a key role in determining the "level of turbulence" of the free-running signal. In Ref. [7], the reduction of the spatial bandwidth to a value of 1.6 (in units of the diffractive wave number of the system) was, *per se*, able to provide a certain degree of control for the hexagonal patterns. However, in that case the value of the pump intensity I normalized to its threshold value I_c for the formation of hexagons was equal to 2, while we here use 3.2. As a result, in our case the simple limitation of the Fourier bandwidth is not sufficient to stabilize any pattern, as witnessed by Figs. 1(b) and 1(c). In what follows, we keep the spatial frequency bandwidth fixed at 1.5.

In order to achieve control over the dynamics, a fraction of the beam traveling on the MOFL is extracted and detected by a video camera, which is interfaced to the PC via a frame grabber. The computer processes the input image, and sends a suitable driving signal to the liquid crystal display device. The LCD transfer function $T(x, y)$ is the sum of a constant mean transfer coefficient T_0, plus a modulation signal $s(x, y)$, chosen to be proportional to the error signal between the current pattern intensity I_{fb} present in the system, and a target pattern $I_T(x, y)$:

$$s(x, y, t) = -\beta[I_{fb}(x, y, t) - I_T(x, y)]. \qquad (2)$$

The operations performed by the PC include the evaluation of the above error signal, and the calculation of the cross-correlation between pattern and target. The refreshing time for the above procedure is at most 200 ms, to be compared to the characteristic time of the pattern dynamics (computed from the decay of the autocorrelation function) which is of the order of the second.

The spatial resolution of the feedback signal is also an important parameter for control. The diffractive scale of the system (the size of the structures visible in Fig. 1(b)] is $\sqrt{2\lambda L} \simeq 300$ μm ($\lambda = 514$ nm being the laser wavelength, and $L = 90$ mm the free propagation length in the MOFL). The selected area for control is of 1200×1200 μm, upon which a control signal of 128×128 pixels is sent. So, a typical (full) wavelength of the pattern is covered by 35–40 pixels, which ensure a good resolution.

The LCD is illuminated with a uniform intensity I_0, and the output beam is imaged onto the rear (writing) side of the valve. Following the above discussion, this beam consists of a constant term $T_0 I_0$ that acts in renormalizing the valve working point ϕ_0 to ϕ_0', plus a modulated controlling beam sI_0. The equation of motion when the control loop is closed is therefore:

$$\frac{\partial \phi}{\partial t} = -\frac{1}{\tau}(\phi - \phi_0') + D\Delta\phi + \alpha[I_{fb} - \gamma(I_{fb} - I_T)], \qquad (3)$$

where $\gamma \equiv \beta I_0$. At an open control loop, for $I/I_c = 3.2$ the evolution brings the system to display a time evolving, spatially disordered pattern, where many defects are continuously created and annihilated within a hexagonal-like pattern, thus generating STC [11]. A typical snapshot of the uncontrolled dynamics is reported in Fig. 1(b). Figure 1(c) reports the space-time dynamical evolution of the central vertical line in Fig. 1(b), showing how the uncontrolled dynamics evolves within STC, with a non stationary complex local dynamics and a decaying spatial correlation.

Starting from these conditions, three different target patterns are selected, namely, perfect hexagons, squares, and a particular snapshot of the uncontrolled dynamical evolution (Fig. 2, top). Perfect stationary hexagons are a stable solution close to the pattern formation threshold; they are destabilized when the pump is increased, resulting in the space-time-chaotic dynamics here considered. Therefore, use of hexagons as a target tests the ability of the method to control an unstable solution.

On the other hand, using as the target a snapshot of the uncontrolled dynamics assesses the robustness of the method to freeze a given natural state of the uncontrolled

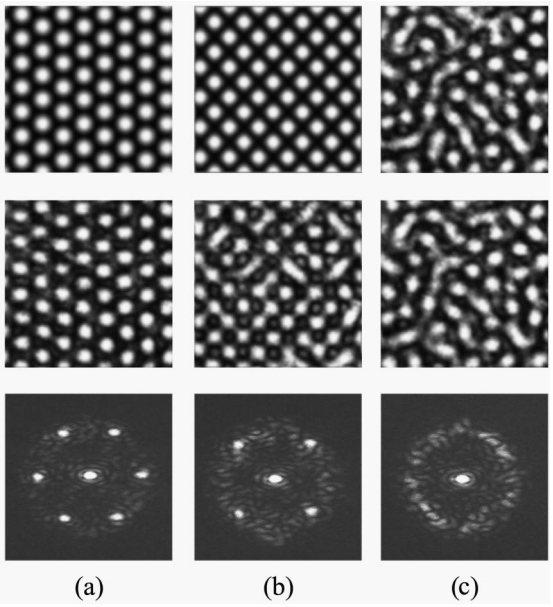

FIG. 2. Examples of target patterns (top row), controlled area in the system at $\gamma = 0.4$ (center row) and corresponding far field images (bottom row) for the control trials of a perfect hexagonal pattern (a), a square pattern (b), and a snapshot of the uncontrolled dynamics (c).

dynamics, in the very same spirit as the so-called targeting of chaos [1]. Finally, squares are never spontaneously selected by the system without control, and therefore they serve us to assess the ability of the control strategy to force the appearance of an arbitrary symmetry. The results obtained for $\gamma = 0.4$ in the three cases are reported in the center row of Fig. 2, indicating that the control procedure is successful in all cases.

The bottom row of Fig. 2 shows the far field images of the controlled dynamics. While hexagonal and square patterns have a simple global symmetry (thus allowing for an easy implementation of Fourier filtering techniques, like the one of Ref. [6]), the target STC snapshot involves the presence of a complicated power spectrum. The fabrication of Fourier masks reproducing the amplitude and phase of these patterns appears extremely difficult in experiments.

By acting directly on the near field patterns, our control method circumvents such practical difficulties, is also effective in stabilizing complex Fourier patterns, and therefore configures as the most reliable choice for the stabilization and targeting of two dimensional stationary structures with arbitrary symmetries and shapes.

To evaluate quantitatively the control ability of our method, we use the time-dependent correlation function $C(t) = \langle I_{fb}(\mathbf{r}, t) \cdot I_T(\mathbf{r}) \rangle_{\mathbf{r}}$ between the instantaneous pattern and the target one ($\langle \ldots \rangle_{\mathbf{r}}$ denotes a spatial average). We also measure the amount of power $p(t) = \gamma \{ \langle [I_{fb}(\mathbf{r}, t) - I_T(\mathbf{r})]^2 \rangle_{\mathbf{r}} \}^{1/2}$ injected within the control arm for controlling the target pattern.

The correlations vs time are shown in Fig. 3 for increasing values of γ for the control task of a perfect hexagonal pattern (a), a snapshot of the uncontrolled dynamics (c), and a square pattern (e). At lower values of γ ($\gamma = 0.1, 0.2$), there is already a partial control of the dynamics, though several deviations of the patterns around the target ones still remain. The correlation value increases with γ up to $\gamma = 0.4$, where a high degree of control is achieved in all cases. As γ increases, the transient time before reaching control over the target pattern decreases. On the opposite, when control is switched off, the relaxing time is determined by the characteristic time of the STC decorrelation, and is therefore independent of γ. Simulations performed evolving Eq. (3) with the set of parameters used in our setup are in quantitative agreement with the experimental observations within few percent.

Notice that the maximum correlation is attained for the case of the STC snapshot. This is due to the fact that in this case the target pattern is a specific configuration of the natural evolution of the dynamics. In the cases of squares and hexagons, instead, the target patterns are digitally generated trying to reproduce at best the natural profile of the spots present in the system; but this procedure is intrinsically imperfect, because the exact profile of the spots is unknown.

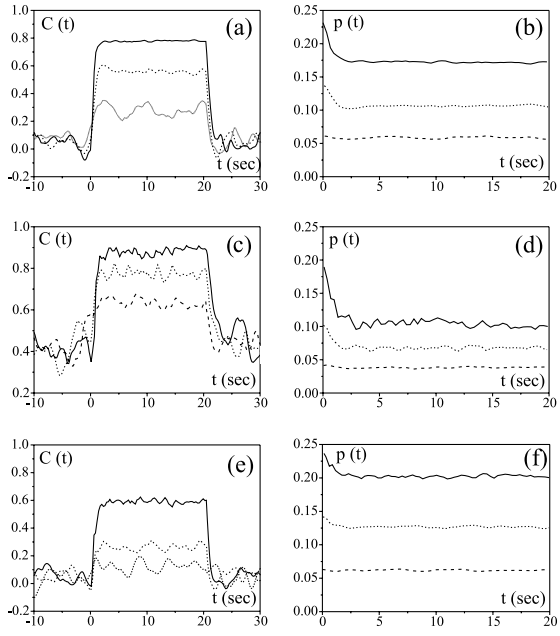

FIG. 3. Correlation function $C(t)$ (a), (c), (e) and amount of power $p(t)$ injected within the control arm (b), (d), (f) vs time (in seconds). The two quantities are defined in the text. In all cases the continuous line refers to $\gamma = 0.4$, the dotted line to $\gamma = 0.2$, and the dashed line to $\gamma = 0.1$. (a), (b) the target is a perfect hexagonal pattern; (c), (d) the target is a snapshot of the uncontrolled dynamics; (e), (f) the target is a perfect square pattern. $I/I_c \simeq 3.2$.

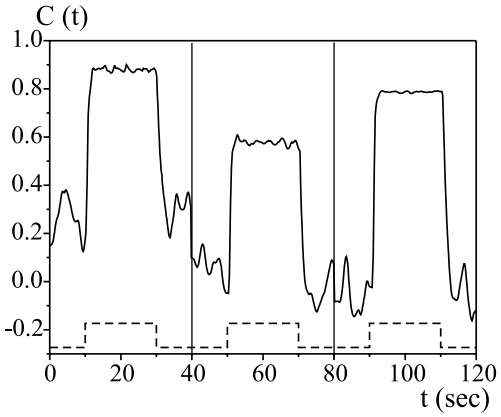

FIG. 4. Correlation function $C(t)$ (see text for definition) vs time during the sequential control trial at $\gamma = 0.4$. The target patterns are a snapshot of the uncontrolled dynamics ($10 \leq t < 30$ sec), a square pattern ($50 \leq t < 70$ sec), and a hexagonal pattern ($90 \leq t < 110$ sec). The dashed line indicates the switching on/off times. The vertical lines separate the three domains in time in which a different pattern is taken as target for the control. In each time domain, the correlation is calculated using the corresponding target pattern.

This is the same reason why the asymptotic values of the power control in Fig. 3(b), 3(d), and 3(f) are increasing function of γ. This power is the product of γ itself, by the root mean square of the error signal, and hence it can go to zero only if the error signal vanishes, which cannot be the case for target patterns that are only approximations of the real solutions. Consistently, the control power needed is substantially lower for the snapshot than for hexagons and squares; the snapshot indeed represents rather closely a natural state of the system, being captured during the spontaneous evolution of the dynamics. However, also in this case, discretization errors and/or other experimental imperfections prevent the error signal from vanishing exactly.

It is worth observing that the correlation when control is off in Fig. 3(c) does not decay to zero; this is due to the fact that our uncontrolled STC dynamics gives rise to a nonzero mean field. This point can be qualitatively appreciated from inspection of Fig. 1(c): the pattern has a certain degree of "phase rigidity", i.e., even if there are chaotic fluctuations, bright (dark) areas remain more or less bright (dark) for most of time. Similar properties have been observed experimentally and discussed in various other cases of space extended systems giving rise to STC dynamics [12].

Finally, we demonstrate that our control technique is flexible in dynamically switching between different target patterns. For this purpose, we prepare a time-dependent target pattern formed by the ordered sequence of a snapshot of the uncontrolled dynamics, a square pattern and a hexagonal pattern, each one presented to the system for a time $T = 20$ sec, and intermingled with periods of $T = 20$ sec of time in which the system is left uncontrolled to reset the original state of STC. The results are shown in Fig. 4, where one sees that the system is able to attain each one of the target patterns in the sequence for the same value of $\gamma = 0.4$, as well as to switch between the different patterns. Notice that each target pattern in the sequence produces a different state in the correlation, as in Fig. 2. The maximal correlation is again obtained for the snapshot of the uncontrolled dynamics, since this pattern represents a specific state compatible with the uncontrolled dynamics.

This work was partly supported by EU Contract No. HPRN-CT-2000-00158, and MIUR-FIRB project no. RBNE01CW3M-001.

[1] For a comprehensive review of the topic see S. Boccaletti, C. Grebogi, Y. C. Lai, H. Mancini, and D. Maza, Phys. Rep. **329**, 103 (2000), and references therein.

[2] I. Aranson, H. Levine, and L. Tsimring, Phys. Rev. Lett. **72**, 2561 (1994); W. Lu, D. Yu, and R. G. Harrison, Phys. Rev. Lett. **76**, 3316 (1996); R. Martin, A. J. Scroggie, G. L. Oppo, and W. J. Firth, Phys. Rev. Lett. **77**, 4007 (1996); N. Baba, A. Amann, E. Schoell, and W. Just Phys. Rev. Lett. **89**, 074101 (2002).

[3] P. Parmananda, M. Hildebrand, and M. Eiswirth, Phys. Rev. E **56**, 239 (1997); R. O. Grigoriev, M. C. Cross, and H. G. Schuster, Phys. Rev. Lett. **79**, 2795 (1997); L. Kocarev, U. Parlitz, T. Stojanovski, and P. Janjic, Phys. Rev. E **56**, 1238 (1997).

[4] R. Montagne and P. Colet, Phys. Rev. E **56**, 4017 (1997); S. Boccaletti, J. Bragard, and F. T. Arecchi, Phys. Rev. E **59**, 6574 (1999).

[5] M. E. Bleich, D. Hochheiser, J. V. Moloney, and E. S. Socolar, Phys. Rev. E **55**, 2119 (1997); D. Hochheiser, J. V. Moloney, and J. Lega, Phys. Rev. A **55**, R4011 (1997).

[6] S. Juul Jensen, M. Schwab, and C. Denz, Phys. Rev. Lett. **81**, 1614 (1998); T. Ackemann, B. Giese, B. Schäpers, and W. Lange, J. Opt. B **1**, 70 (1999); G. K. Harkness, G. L. Oppo, E. Benkler, M. Kreuzer, R. Neubecker, and T. Tschudi, J. Opt. B **1**, 177 (1999); E. Benkler, M. Kreuzer, R. Neubecker, and T. Tschudi, Phys. Rev. Lett. **84**, 879 (2000).

[7] A. V. Mamaev and M. Saffman, Phys. Rev. Lett., **80**, 3499 (1998).

[8] S. A. Akhmanov, M. A. Vorontsov, and V. Yu Ivanov, JETP Lett. **47**, 707 (1988).

[9] G. P. D'Alessandro and W. J. Firth, Phys. Rev. Lett. **66**, 2597 (1991).

[10] R. Neubecker, G. L. Oppo, B. Thuering, and T. Tschudi, Phys. Rev. A **52**, 791 (1995).

[11] R. Neubecker, B. Thuring, M. Kreuzer, and T. Tschudi, Chaos Solitons Fractals **10**, 681 (1999).

[12] B. J. Gluckman, P. Marcq, J, Bridger, and J. P. Gollub, Phys. Rev. Lett. **71**, 2034 (1993); Li Ning, Y. Hu, R. E. Ecke, and G. Ahlers, Phys. Rev. Lett. **71**, 2216 (1993).